THE JOURNAL OF PHYSICAL CHEMISTRY C

Article

pubs.acs.org/JPCC

Thermal and Photochemical Reactions of Methanol, Acetaldehyde, and Acetic Acid on Brookite TiO_2 Nanorods

Paul A. Pepin,*[,†] Benjamin T. Diroll,[‡,∥] Hyuck J. Choi,[†,‡] Christopher B. Murray,[‡,§] and John M. Vohs*[,†]

[†]Department of Chemical and Biomolecular Engineering, [‡]Department of Chemistry, and [§]Department of Materials Science and Engineering, University of Pennsylvania, Philadelphia, Pennsylvania 19104, United States

Supporting Information

ABSTRACT: The catalytic and photocatalytic activity of brookite TiO_2 nanorods toward methanol, acetaldehyde, and acetic acid was studied using temperature-programmed desorption (TPD). For thermally activated reactions, the brookite nanorods were found to exhibit catalytic properties similar to those reported previously for the rutile and anatase phases of TiO_2. In particular, methanol adsorbed dissociatively on 5-fold coordinate surface Ti cations and underwent dehydrogenation to formaldehyde and deoxygenation to methane near 650 K; acetaldehyde adsorbed on these sites underwent aldol condensation to produce crotonaldehyde and to a lesser extent reductive coupling to butene between 460 and 600 K; acetic acid adsorbed dissociatively to produce acetate species that decomposed to produce ketene at 630 K. The brookite nanorods were also found to be photocatalytically active for the coupling of methanol to methyl formate and the photo-oxidation of acetaldehyde to acetate. Lastly, the photocatalytic activity of the brookite nanorods was found to be length-dependent, with longer rods exhibiting higher activity. This length dependence is attributed to enhanced delocalization of the photoexcited electrons in the longer rods, thereby decreasing the rate of electron−hole recombination.

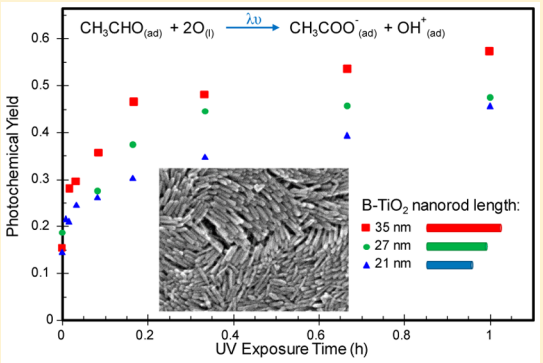

1. INTRODUCTION

Photocatalytic materials have the potential for a wide range of applications, including the storage of solar energy through chemical transformations such as water-splitting, air and water purification, and providing alternative low-energy reaction pathways for conventional industrial thermochemical processes. TiO_2 is a prototypical photocatalyst which is active for many of these reactions. It has a bandgap of ∼3 eV, such that it adsorbs light in the ultraviolet (UV) region of the spectrum, and has been the subject of numerous investigations. Of the three naturally occurring polymorphs of titania, rutile (R-TiO_2), anatase (A-TiO_2), and brookite (B-TiO_2), the former two have received the most attention, and the relationships between reactivity, surface structure, and in some cases bulk crystallite size and shape have been elucidated for a variety of catalytic and photocatalytic reactions.[1−19] In this regard, studies employing single crystals or epitaxial thin films of these materials have provided much insight into how the local atomic structure of TiO_2 surfaces affect activity.[1−11] The reader is referred to several excellent review articles that describe this body of work.[17−19]

In contrast to R-TiO_2 and A-TiO_2, little is currently known about the catalytic and photocatalytic properties of the metastable brookite phase which has, until recently, proven difficult to synthesize in its pure form. The development of synthesis procedures for B-TiO_2, however, have now motivated studies of its catalytic properties. For example, Li et al.[20] as well as Murikami et al.[21] have studied the reactivity of B-TiO_2 nanoparticles synthesized using a hydrothermal method and observed that they are highly active for the photodecomposition of acetaldehyde under various conditions. Other recent studies have investigated the effect of bulk particle size on the photocatalytic activity of B-TiO_2 nanocrystals.[22,23] For example, Ohno et al. studied photocatalytic oxidation of acetaldehyde to CO_2 in air over B-TiO_2 nanorods of various aspect ratios both with and without an Fe^{3+} dopant. They observed that the photocatalytic activity was aspect ratio dependent, with higher aspect ratios displaying higher activity.[22] Similarly, Cargnello et al. have recently reported that the aqueous phase photoreforming of ethanol to produce H_2 over B-TiO_2 nanorods decorated with Pt nanoparticles exhibits a strong length dependence. They attributed this trend to enhanced separation of photogenerated electrons and holes in longer nanorods which increases the probability that the holes will diffuse to an exposed surface and react with adsorbates prior to electron−hole recombination.[23]

The aim of the present study was twofold: first to investigate the adsorption and thermally induced reactions of the simple

Received: March 20, 2017
Revised: May 4, 2017
Published: May 9, 2017

DOI: 10.1021/acs.jpcc.7b02615
J. Phys. Chem. C 2017, 121, 11488−11498

oxygenates, methanol, acetaldehyde, and acetic acid, on the brookite phase of titania and to compare this reactivity to what has previously been observed for the R-TiO_2 and A-TiO_2 phases, and second to investigate the photocatalytic activity of the brookite phase for both the oxidation and the reductive coupling of oxygenates. Size-selected B-TiO_2 nanorods were used in the study, thereby allowing us to also further investigate the effect of nanorod length on photocatalytic activity.

2. MATERIALS AND METHODS

B-TiO_2 nanorods were synthesized using the method described in detail by Buonsanti et al.[24] The procedure consisted of initially combining 10 mL of oleylamine (70%, Sigma-Aldrich), 10 mL of octadecene (90%, Acros), and 0.5 mL of oleic acid (90%, Sigma-Aldrich) followed by heating under vacuum at 393 K for 1 h and then cooling to 333 K under nitrogen flow. Then, 1.5 mL of titanium precursor solution [75 mL of 0.2 M, of octadecene, 23.6 mL oleic acid, and 1.65 mL titanium tetrachloride (99.9%, Acros)] was injected followed by heating to 563 K. After the sample was held at this temperature for 10 min, additional titanium precursor solution was dropwise added at a rate of 0.3 mL min^{-1}. The reaction flask was then allowed to cool to 323 K. The size of the nanorods was controlled by adjusting the volume of the dropwise added solution. Three separate B-TiO_2 rod lengths, 21, 27, and 35 nm, were used in this study. The standard deviation of the rod lengths for each sample was 1.4, 2.2, and 3.1 nm, respectively.

Purification of the nanorods was performed by adding 10 mL of toluene to the reaction flask and centrifuging at 8000 rpm for 5 min. The precipitate was redispersed as a clear solution in toluene mixed with 100 μL of oleylamine to improve solubility then precipitated again with isopropanol. Further washing in hexane was used to remove any excess organic material. The band gap of similarly fabricated B-TiO_2 nanorods has been measured previously by Cargnello et al. using diffuse-reflectance ultraviolet−visible (UV−vis) spectroscopy and found to be 3.4 eV and independent of rod length.[23] This value is slightly greater than that of the anatase and rutile phases.

A-TiO_2 nanoparticles with a platelet morphology were also synthesized using a procedure similar to that for synthesis of the nanorods, which is described in detail by Gordon et al.[25] The nanoplatelets were measured to be 18 nm across using scanning electron microscopy (SEM) as described below. The reactivity of CH_3OH on these nanocrystals has been studied extensively and reported by Bennett et al.[14] In this study, we again employed these platelet nanocrystals for comparative purposes to study the dependence of reactivity of CH_3CHO and CH_3COOH on surface structure.

Temperature-programmed desorption (TPD) was used to characterize the reactivity of both powder and thin-film samples. B-TiO_2 nanorod thin films that were used for TPD studies carried out in ultrahigh vacuum (UHV) were prepared by drop-casting the B-TiO_2 nanorods dissolved in hexane onto an oxidized silicon wafer. After the solvent was allowed to evaporate, each sample was placed in a UV−ozone cleaner for 3 h to remove surface-bound ligands. Powder samples were prepared by dissolving the B-TiO_2 nanorods in a biphasic mixture of hexane and dimethylformamide to which nitrosonium tetrafluoroborate was added at an equivalent weight ratio to the nanorods. The mixture was shaken vigorously, and the particles were flocculated using toluene and acetonitrile. An additional washing step was performed by dissolving the sample in dimethylformamide and precipitating again with toluene. The precipitate was dried overnight in a vacuum oven at 363 K, and the resulting white solid was ground to a fine powder using a mortar and pestle.

A high-vacuum TPD, thermogravimetric analysis (TGA) instrument was used to characterize the reactivity of oxygenates on the unsupported B-TiO_2 nanorod samples and to determine the coverage of adsorbed intermediates. The turbo-pumped system consisted of a microbalance (Parr Instrument Co.) in which the sample was held in a tantalum holder suspended in a quartz tube. The sample was heated radiantly by an external heating element. The temperature was measured using a type-K thermocouple in contact with the quartz tube. The vacuum system also housed a quadrupole mass spectrometer (Stanford Research Systems) which was used to monitor desorption products during TPD experiments and a dosing manifold for admitting controlled amounts of reactant gases into the vacuum chamber. Fresh powder samples were initially heated in vacuum to 523 K to remove adsorbed species. In a typical TPD/TGA experiment, the sample was exposed to the reactant vapor followed by evacuation to less than 1×10^{-8} Torr for 1 h to remove any condensed species. The sample was then heated at 10 K min^{-1} up to 773 K while monitoring its mass and the desorbing species using the mass spectrometer.

TPD experiments for the thin-film B-TiO_2 samples were conducted using an UHV chamber equipped with a quadrupole mass spectrometer (Stanford Research Systems) and an electron gun and electron energy analyzer for performing Auger electron spectroscopy (AES). The UHV system was also equipped with a 365 nm UV LED monochromatic light source (Prizmatix) connected via fiber optic cables and feedthrough to facilitate illuminating a sample with UV light. Reactants, CH_3OH (99.9%, Fisher Scientific), CH_3CH_2O (99.5%, Acros), and CH_3COOH (99.9%, Fisher Scientific) were admitted into the chamber using a dosing manifold that was connected to the main UHV chamber with a variable leak valve equipped with a dosing needle to direct the flux of reactant to the sample surface. The reactants were degassed using repeated freeze−pump−thaw cycles prior to use. A separate UHV chamber equipped with an X-ray source (VG Microtech) and a hemispherical electron energy analyzer (Leybold-Heraeus) was used for X-ray photoelectron spectroscopy (XPS) measurements. All XPS spectra were referenced to the Ti($2p_{3/2}$) peak for Ti^{4+} at 459.3 eV.[26]

For UHV TPD measurements, a 5 mm × 7 mm silicon wafer-supported B-TiO_2 sample was mounted in a tantalum foil folder that was attached to an electrical feedthrough on the UHV sample manipulator. The temperature was monitored using a type-K thermocouple which was attached to the back of the silicon wafer using a ceramic adhesive (Aremco). The sample could be cooled by conduction from a liquid N_2 reservoir on the manipulator and heated resistively up to 800 K. For a TPD experiment, the sample was initially positioned in front of the dosing needle on the leak valve and exposed to the desired amount of reactant. The sample was then positioned in front of the mass spectrometer and heated at 3 K s^{-1} while recording the desorption products.

TPD was also used to characterize the photocatalytic activity of the B-TiO_2 nanorods. In these experiments, after being dosed with the desired reactant, the sample was positioned in front of the fiber optic cable connected to the UV source and illuminated with UV light for a set time. The photon flux from the UV source at the sample surface was $\sim 10^{15}$ cm^{-2} s^{-1} as determined using a Thorlabs photodiode detector. The sample

DOI: 10.1021/acs.jpcc.7b02615
J. Phys. Chem. C 2017, 121, 11488−11498

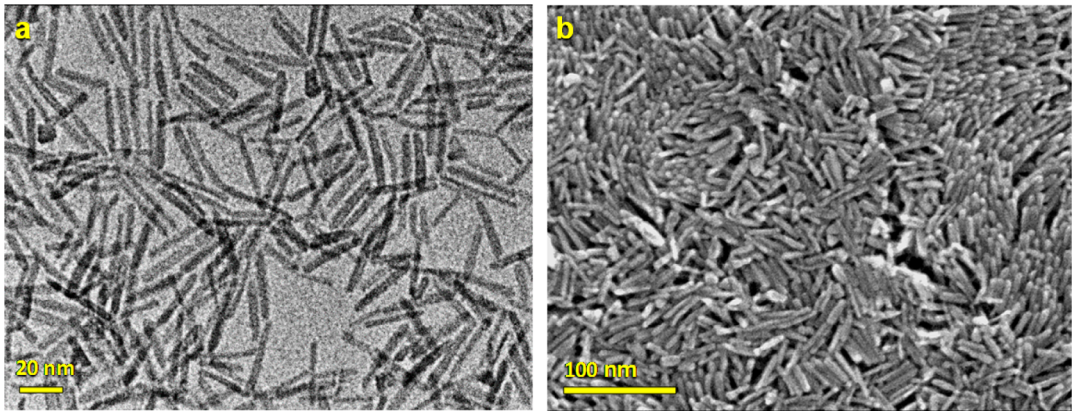

Figure 1. (a) TEM micrographs of the as-synthesized 27 nm nanorods and (b) SEM micrograph of a thin film of the 35 nm nanorods on an oxidized Si substrate.

was maintained at 165 K during reagent dosing and UV illumination to prevent reagent desorption. After UV illumination, the sample was repositioned in front of the mass spectrometer and TPD experiments were conducted by heating the sample at a rate of 3 $K s^{-1}$ and recording the desorption products.

Desorption products during TPD experiments for both the HV and UHV systems were identified by their characteristic mass spectrometer fragmentation patterns. Multiple mass-to-charge ratios were monitored in each TPD run to ensure proper identification of all products. All reported TPD spectra have been corrected for any overlap in cracking patterns and have been scaled to adjust for the mass spectrometer sensitivity factors for each product.

Transmission electron microscopy (TEM) was used to characterize the as-synthesized nanocrystals. For TEM characterization, the nanocrystals were dispersed onto a 300 mesh C-coated Cu TEM grid, and images were collected using a JEOL JEM1400 TEM operating at 120 kV. The drop-cast thin-film samples to be used for UHV studies were characterized by scanning electron microscopy using a JEOL 7500F HRSEM. For SEM characterization, the thin-film samples were not coated, but a conducting tape was applied near the edge of the substrate to prevent sample charging. Images were collected with a 5 kV beam.

3. RESULTS

3.1. Catalyst Characterization. As previously mentioned, TEM and SEM were used to characterize the as-synthesized brookite nanorods as well as the drop-cast films used in this study. These techniques revealed that each nanorod sample was highly monodisperse. As noted above, three separate nanorod batches, which had lengths of 21, 27, and 35 nm, were used in this study. A TEM image of the as-synthesized 27 nm brookite nanorods and a SEM image of a freshly cast film of these rods is displayed in Figure 1. SEM images were also obtained for the thin films after completion of reactivity studies (typically between 30 and 50 TPD experiments per sample) and confirmed the stability of the films with no sintering of the nanocrystals being observed. For all nanorod samples, the diameter of the nanorods was observed to be ~5.5 nm. Using these measured dimensions of the nanorods and the bulk density of brookite (4.14 g cm^{-3}),[27] the surface area of the nanorods was calculated to be 175 $m^2 g^{-1}$. Although accurate Brunauer–Emmett–Teller (BET) measurements from these samples were not possible because of the small quantities obtained from the synthesis, BET measurements conducted by Cargnello and co-workers for similarly fabricated nanorods are in close agreement with these calculated values.[23]

XPS was used to characterize the surface composition and the Ti oxidation state in the nanorods. Ti(2p) and O(1s) spectra for the 27 nm thin film obtained after annealing in 2×10^{-8} Torr of O_2 at 750 K (see Figure S1) contained peaks at 465.5 and 459.3 eV, which are characteristic of the $2p_{1/2}$, $2p_{3/2}$ doublet for Ti^{4+}, indicating that the Ti in the nanorods is fully oxidized. XPS was also used to check for both C and Cl impurities which may result from the synthesis procedure, but neither were detected, demonstrating that the ligand removal methods and O_2 annealing treatment were sufficient to produce clean surfaces.

3.2. Thermally Induced Reactions of Simple Oxygenates on Brookite Nanorods. To provide base case data for the photochemical reactivity studies and to explore the reactivity of brookite surfaces toward simple oxygenates, TPD experiments for the reaction of CH_3OH, CH_3CHO, and CH_3COOH on the nanorods in the dark were initially performed. TPD experiments were performed with each reagent for the 21, 27, and 35 nm B-TiO_2 nanorods. No effects due to length were observed, indicating that the nanorod ends do not exhibit activity that is noticeably different from the nanorod sides. Given the large aspect ratios of the nanorods used in this study, this result suggests that the majority of the active sites are on the nanorod sides. Thus, we report TPD data only for a single rod length in this section.

3.2.1. Methanol Thermal Chemistry. TPD experiments as a function of the CH_3OH exposure were initially performed to determine the dose required to obtain saturation coverage. Methanol desorption curves as a function of exposure for the 21 nm thin film are displayed in Figure 2. For doses up to 5 L at a sample temperature of 165 K, the spectra contain two peaks: a large broad peak centered at 330 K and a smaller sharper peak centered at 640 K. The low-temperature peak can be assigned to desorption of weakly bound molecular CH_3OH while, as will be shown below, the high-temperature peak is a product of the reaction of adsorbed methoxide species. Thus, CH_3OH adsorbs both molecularly and dissociatively on the brookite surface. Further increasing the CH_3OH exposure resulted in a continued increase in the peak intensities and the emergence of a new peak at ~250 K, which is consistent with desorption of CH_3OH multilayers. For CH_3OH doses up to 10 L, saturation

DOI: 10.1021/acs.jpcc.7b02615
J. Phys. Chem. C 2017, 121, 11488–11498

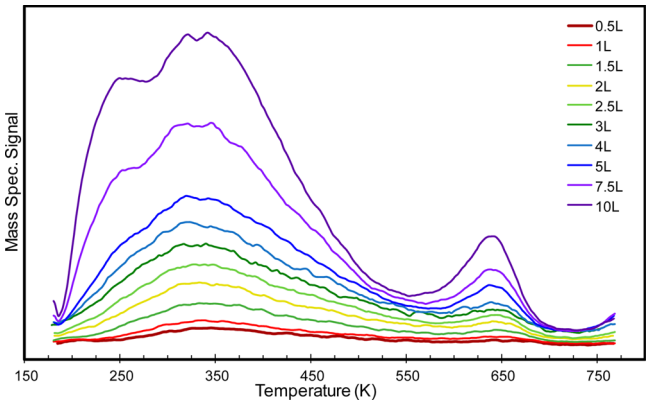

Figure 2. Methanol TPD spectra from 21 nm B-TiO_2 nanorod thin-film sample for various methanol doses as indicated in the figure.

of the thin film was not achieved, but it was observed that the ratio of the areas of the high- and low-temperature (330 K) peaks remained relatively constant throughout the dosage range. Because the thin films contain multiple layers of nanorods, we believe that the outermost layer of the nanorods are initially being saturated followed by CH_3OH penetrating deeper into the film at higher doses. Because of the need to use very large exposures, it was not practical to saturate the entire film with the oxygenate reactant; however, because the ratio of the peaks remained constant, the TPD results appear to be largely independent of CH_3OH coverage. We therefore chose to use a 5 L CH_3OH dose in more detailed methanol reactivity studies.

While it was not practical to saturate the entire brookite film in the UHV studies, it was possible to do so using unsupported brookite nanorod powder samples in our high-vacuum TPD/TGA system. As shown in Figure S2, the methanol TPD results from the powder sample are consistent with those from the thin films and contain both low- and high-temperature methanol desorption features. The TGA data in Figure S2 also allow the saturation coverage of adsorbed CH_3OH per unit surface area, 2.4 molecules nm^{-2}, to be determined. This value is comparable with those reported for CH_3OH on A-TiO_2 powders which range from 2.25 to 3.18 molecules nm^{-2},[1,28−30] while reported values for R-TiO_2 powders are somewhat higher, ranging from 4.62 to 4.76 molecules nm^{-2}.[30,31]

In addition to CH_3OH, the reaction products H_2O, CH_4, CH_2O, and CH_3OCH_3 were also observed during TPD. Figure 3a displays the TPD product desorption peaks obtained from a 21 nm thin film dosed with 5 L of CH_3OH at 165 K. As mentioned in Materials and Methods, the desorption intensities for each product have been corrected for their respective mass spectrometer sensitivity factors allowing for quantitative comparison of the product yields. Water appears in a large peak at 390 K and a much smaller feature at 650 K. The H_2O produced at 390 K can be attributed to the reaction of surface hydroxyl species which were formed during dissociative adsorption of CH_3OH. While the majority of the resulting adsorbed methoxy groups recombine with the adsorbed H to form CH_3OH which desorbs below 500 K, H_2O production is a competing pathway that results in some of the methoxy groups becoming "stranded" on the surface. These methoxy groups react primarily via two different pathways to produce the products that appear at high temperatures. One is a dehydrogenation−disproportionation pathway that produces formaldehyde at 650 K and hydroxyl groups which can

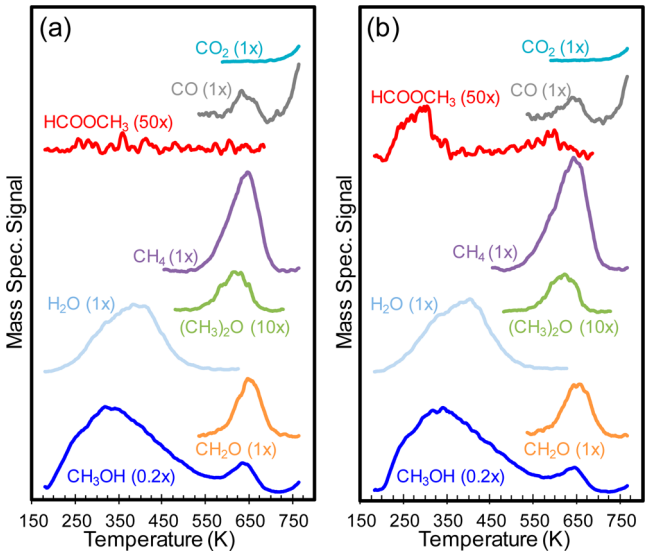

Figure 3. TPD spectra obtained from 21 nm B-TiO_2 nanorods following 5 L CH_3OH dose at 165 K: (a) no UV exposure and (b) 1 h UV exposure.

combine with remaining adsorbed methoxy groups, giving rise to the high-temperature CH_3OH peak at 640 K. The second is deoxygenation to produce methane at 650 K. Some bimolecular coupling of adsorbed methoxy groups is also observed as a minor pathway producing a small amount of dimethyl ether near 640 K. Note that these TPD peak assignments are similar to those reported by the Barteau group for the reaction of CH_3OH on A-TiO_2 powders.[1]

Studies of the reaction of CH_3OH on R-TiO_2 single crystals have determined that the dimethyl ether product results from the coupling of two methoxy species that are adsorbed on a common Ti cation site.[1,2,30] Thus, the active sites for this reaction are surface Ti cations with multiple coordination vacancies. The observation that the fractional yield of dimethyl ether for the brookite nanorods was quite small (less than 3% of the high-temperature reaction products) therefore implies that the surfaces of these nanorods contain few such sites.

As noted above, the brookite nanorod length did not affect the thermally induced reactions of adsorbed CH_3OH. It is useful, however, to compare the observed CH_3OH reactivity on the brookite nanorods with that reported previously for A-TiO_2 powders and nanocrystals. Figure 4 compares the fractional yields for the primary reaction products obtained during CH_3OH TPD experiments with the brookite nanorods used in the present study to those reported previously for a polycrystalline A-TiO_2 powder[1] and a thin film of 18 nm A-TiO_2 nanocrystals that had a platelet morphology which predominantly exposes the (001) surface.[14] The product yields for the two A-TiO_2 samples are qualitatively similar and show that all three competing pathways for the reaction of methoxy groups, i.e., dehydrogenation to formaldehyde, coupling to dimethyl ether, and deoxygenation to methane, occur to comparable extents on these samples. This is in contrast to the brookite nanorods on which deoxygenation to methane predominates and coupling to dimethyl ether is only a minor pathway. The latter is consistent with our conclusion that the surfaces of the B-TiO_2 nanorods contain few Ti cations with multiple coordination vacancies which are the active sites for the coupling reaction.

DOI: 10.1021/acs.jpcc.7b02615
J. Phys. Chem. C 2017, 121, 11488−11498

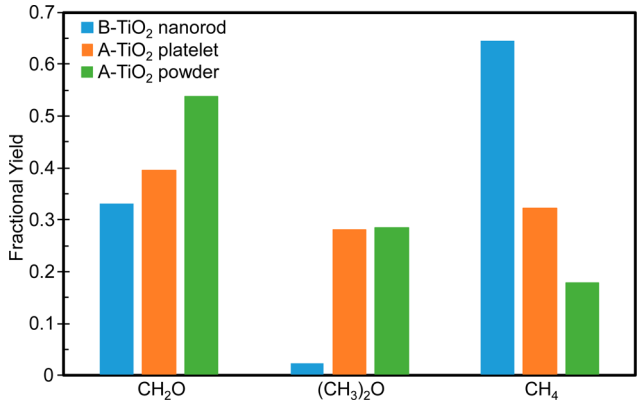

Figure 4. Fractional yields of oxygenate products during CH_3OH TPD for B-TiO_2 nanorods (21 nm), A-TiO_2 platelets (18 nm), and polycrystalline A-TiO_2 powder (A-TiO_2 powder data from ref 1).

3.2.2. Acetaldehyde Thermal Chemistry. Coverage variation TPD experiments with CH_3CHO were also performed on the B-TiO_2 nanorods, and a 5 L dose was again found to be sufficient to saturate the outermost layer of the thin film. Figure 5a displays TPD results obtained for a 21 nm film following a 5

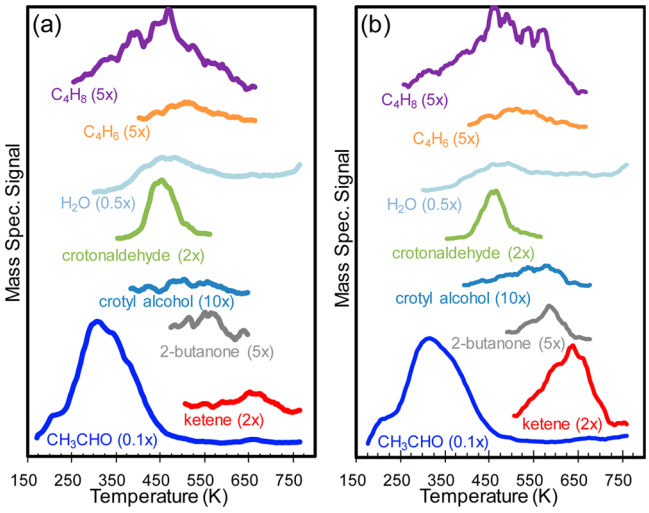

Figure 5. TPD spectra obtained from 21 nm B-TiO_2 nanorods following 5 L CH_3CHO dose at 165 K: (a) no UV exposure and (b) 1 h UV exposure.

L dose of CH_3CHO. The TPD spectra are dominated by a large CH_3CHO desorption peak centered at 290 K, indicating that the B-TiO_2 nanorods have relatively low reactivity toward this molecule. However, small amounts of a range of coupling products were produced, including crotonaldehyde at 460 K. The fact that water was also produced at this temperature is consistent with an aldol condensation pathway. A small amount of crotyl alcohol also desorbed between 540 and 600 K, which likely results from the reduction of a portion of the crotonaldehyde product. Reductive coupling products (butene, butadiene, and 2-butanone) were also observed in small quantities from 450 to 600 K, as was a small amount of the dehydrogenation product, ketene ($CH_2{=}C{=}O$), at 630 K. It is notable that the complete oxidation products, CO and CO_2, were not produced from reaction of CH_3CHO on the nanorods.

The saturation coverage of adsorbed CH_3CHO on the B-TiO_2 nanorods was again estimated using high-vacuum TPD/TGA data obtained from an unsupported nanorod sample (see Figure S3). Using this TGA data, the saturation coverage of CH_3CHO per unit surface area was calculated to be 1.8 molecules nm^{-2}, which is similar to that obtained for CH_3OH, indicating that these two oxygenates adsorb on the same sites.

The CH_3CHO TPD results are similar to those reported previously for reaction of CH_3CHO on various R-TiO_2 and A-TiO_2 single crystal and powder samples.[7,32−36] This similarity is demonstrated in Figure 6, which compares the fractional yield

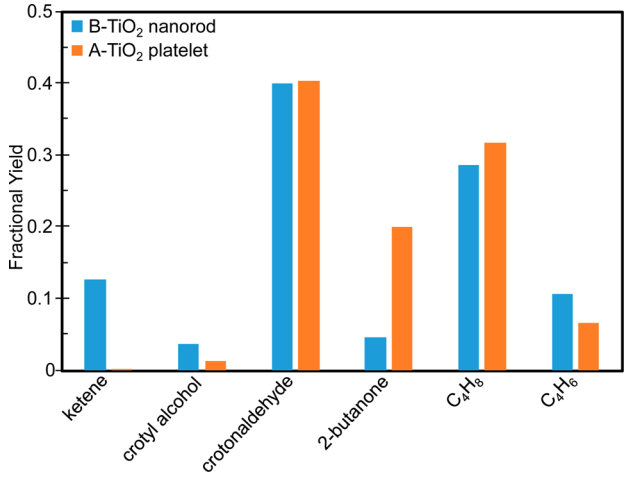

Figure 6. Fractional yields of oxygenate products during CH_3CHO TPD for B-TiO_2 nanorods (21 nm) and A-TiO_2 platelets (18 nm).

of the carbon-containing reaction products during CH_3CHO TPD obtained from the B-TiO_2 nanorod film and from a thin film composed of 18 nm A-TiO_2 platelets. While similar products were produced on both samples, it is noteworthy that ketene was produced only on the B-TiO_2 nanorods.

3.2.3. Acetic Acid Thermal Chemistry. The B-TiO_2 nanorods were found to be highly active for the dehydration of CH_3COOH to produce ketene. As shown in Figure 7, the TPD results obtained from a 21 nm nanorod thin film dosed with 5 L of CH_3COOH (this dose was again found to be

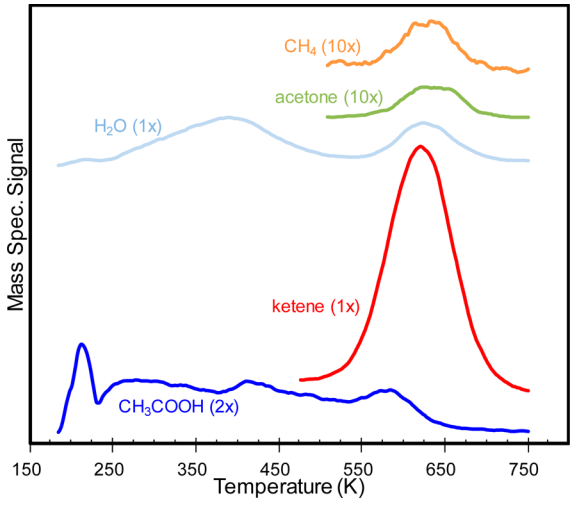

Figure 7. TPD spectra obtained from 21 nm B-TiO_2 nanorods following 5 L CH_3COOH dose at 165 K.

DOI: 10.1021/acs.jpcc.7b02615
J. Phys. Chem. C 2017, 121, 11488−11498

sufficient to saturate the outermost layers of the film) was dominated by a large ketene peak at 630 K. Small amounts of methane and acetone were also produced near this temperature. It is likely that CH_3COOH dissociates on B-TiO_2 to form adsorbed acetate species which react at 630 K to form ketene. These results are similar to those reported previously by Kim and Barteau for the reaction of CH_3COOH on R-TiO_2(001) and A-TiO_2 powder.[1,10] TPD/TGA of CH_3COOH-dosed unsupported B-TiO_2 nanorods (see Figure S4) was again used to estimate the saturation coverage of adsorbed CH_3COOH (or acetate). These data gave a value of 1.1 molecules nm^{-2}, which is roughly half that obtained for CH_3OH, suggesting that acetate species adsorb in a bridged configuration with the oxygens bonding to two adjacent Ti cations.

Figure 8 compares the TPD fractional yield of carbon-containing products during CH_3COOH TPD from the 18 nm

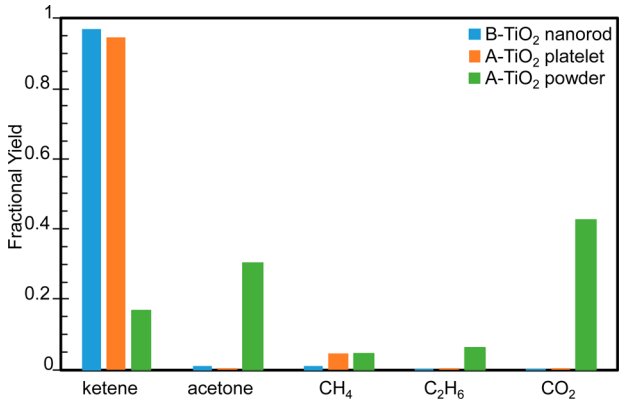

Figure 8. Fractional yields of oxygenate products during CH_3COOH TPD for B-TiO_2 nanorods (21 nm), A-TiO_2 platelets (18 nm), and polycrystalline A-TiO_2 powder (A-TiO_2 powder data from ref 37).

B-TiO_2 nanorod thin film, 18 nm A-TiO_2 platelets thin film, and previously reported values for A-TiO_2 powder.[37] The product yields for the B-TiO_2 nanorods and A-TiO_2 platelets, which preferentially expose the (001) surface, are nearly identical with greater than 90% selectivity to ketene, while those for the A-TiO_2 powder are somewhat different with a high selectivity toward bimolecular coupling to acetone.

3.3. Photochemical Reactions of Simple Oxygenates on Brookite Nanorods. TPD was also used to assess the photocatalytic activity of the B-TiO_2 nanorods. As noted in Materials and Methods, in these experiments the sample at 165 K was dosed with the reactant and then illuminated with the UV light for a specified amount of time, followed by TPD. In addition to exploring the photocatalytic activity of the brookite phase of TiO_2, a goal of these studies was to evaluate how the nanorod length affected photocatalytic activity. Acetic acid was found to not undergo any photochemical reactions on the B-TiO_2 nanorods, so in this section we report results for only CH_3OH and CH_3CHO.

3.3.1. Methanol Photochemistry. Figure 3b displays TPD data obtained after the 21 nm B-TiO_2 nanorod thin-film sample was exposed to 5 L of CH_3OH and then illuminating the sample with 365 nm UV light for 1 h. These data are similar to those obtained without UV illumination (Figure 3a), with CH_2O, $(CH_3)_2O$, CH_4, and CO being produced between 610 and 650 K; however, an additional product, methyl formate ($HCOOCH_3$), resulting from a photochemical coupling pathway, is also observed at 280 K, along with a much smaller peak at 580 K. Note that because the UV illumination occurred with the sample at 165 K, the methyl formate peaks are due to desorption or reaction of surface species that are formed by photochemical reactions that occur at this temperature. The peak at 280 K is most likely desorption-limited and corresponds to methyl formate produced during UV illumination at the lower temperature. The surface species giving rise to the high-temperature peak is less clear. The photochemical nature of these products is further demonstrated by the $HCOOCH_3$ desorption curves as a function of UV exposure displayed in Figure 9. These spectra were obtained from the 21 nm B-TiO_2

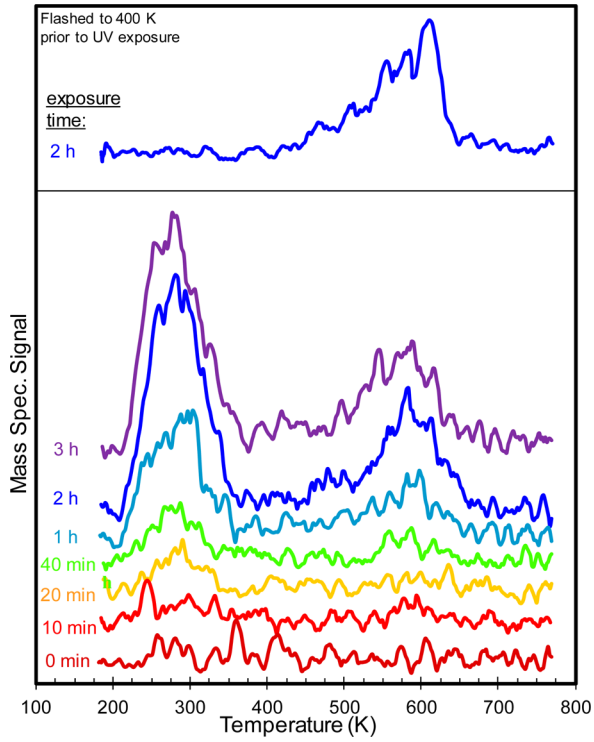

Figure 9. Methyl formate desorption spectra obtained from B-TiO_2 nanorods (21 nm) following 5 L CH_3OH dose at 165 K. Lower panel shows data obtained as a function of the duration of the UV exposure. For the spectrum in the upper panel, the sample was flashed to 400 K following CH_3OH exposure, allowed to cool, and then exposed to UV light for 2 h prior to TPD.

nanorod thin-film sample and show that the intensity of both $HCOOCH_3$ peaks increase with increasing UV exposure for exposures up to 2 h, at which point they become saturated. Note that the $HCOOCH_3$ peak at 280 K is consistent with that observed previously for thin films of A-TiO_2 platelet and bipyramidal nanocrystals which preferentially expose (001) and (101) surfaces,[14] and for R-TiO_2(110) single-crystal surfaces,[5,6] while the higher-temperature peak at 580 K was not observed for these A-TiO_2 and R-TiO_2 samples.

To provide more insight into the photocoupling pathway, the following experiment was performed: A 35 nm B-TiO_2 nanorod thin-film sample was dosed with 5 L of CH_3OH at 165 K, followed by flashing to 400 K to remove all of the weakly bound molecular species, leaving a surface covered with only methoxy groups. The sample was then allowed to cool back to 165 K and illuminated with the UV light for 2 h, and then TPD data were collected. The resulting $HCOOCH_3$ desorption

DOI: 10.1021/acs.jpcc.7b02615
J. Phys. Chem. C 2017, 121, 11488−11498

spectrum is displayed in the upper portion of Figure 9. Note that in this case the spectrum contains only the high-temperature $HCOOCH_3$ peak. The absence of the low-temperature peak at 280 K indicates that the photocoupling reaction that produces this methyl formate product requires the presence of molecularly adsorbed CH_3OH on the surface. In contrast, the high-temperature $HCOOCH_3$ must result from desorption or decomposition of a surface species formed by a photochemical reaction involving only methoxide groups.

The effect of the B-TiO_2 nanorod length on the photocatalytic activity for the coupling of CH_3OH to produce methyl formate was also investigated. The fractional yield (based on the carbon-containing products) of the low-temperature $HCOOCH_3$ product during CH_3OH TPD (5 L dose at 165 K) as a function of the nanorod length and UV exposure time is displayed in Figure 10. These data show that within

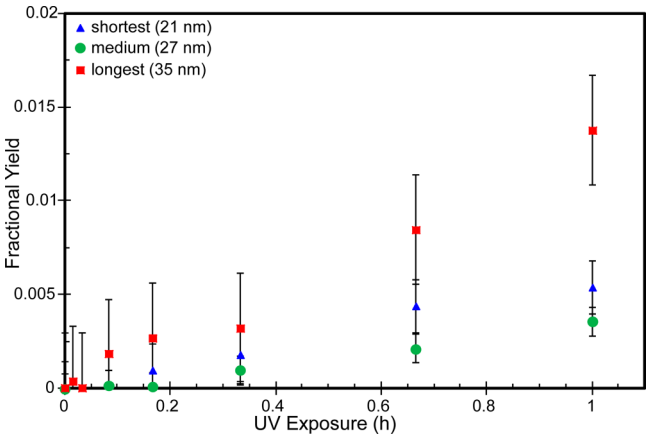

Figure 10. Fractional yield of low-temperature methyl formate product during methanol TPD (5 L dose) as a function of UV exposure and B-TiO_2 nanorod length.

experimental uncertainty there is little difference in the fractional yield for the low-temperature $HCOOCH_3$ product between the 21 and 27 nm rods; however, the 35 nm rods show higher photoactivity for production of the low-temperature $HCOOCH_3$ product. The fractional yield of the high-temperature $HCOOCH_3$ product as a function of nanorod length and UV exposure time exhibited behavior similar to that of the low-temperature $HCOOCH_3$ product (see Figure S5). These data suggest that the photocatalytic activity may increase with increasing rod length, although they are not definitive on this.

3.3.2. Acetaldehyde Photochemistry. Figure 5b displays TPD data obtained after exposing the 21 nm B-TiO_2 nanorod sample to 5 L of CH_3CHO and then illuminating with 365 nm UV light for 1 h. Comparing this TPD data with that obtained with no UV exposure (Figure 5a) reveals that UV illumination causes several changes in the spectra, including a 5-fold increase in the area of the ketene peak at 630 K. This increase in ketene production appears to be at the expense of the crotonaldehyde product, whose peak area decreased by 26% after UV exposure. UV exposure also resulted in small increases of the yield of 2-butanone and butadiene.

Note that the ketene peak temperature, 630 K, is the same as that obtained from CH_3COOH-dosed samples, indicating that they are both due to decomposition of the same surface intermediate. As noted above, in the case of the CH_3COOH reactant, the ketene product almost certainly results from decomposition of an adsorbed acetate species. Thus, the large increase in the ketene yield upon exposure of the CH_3CHO-dosed sample to UV light demonstrates that the B-TiO_2 nanorods have high activity for the photo-oxidation of CH_3CHO to acetate.

This high activity for photo-oxidation of adsorbed CH_3CHO to acetate provides a good test reaction for exploring the effect of the nanorod length on photocatalytic activity. Figure 11

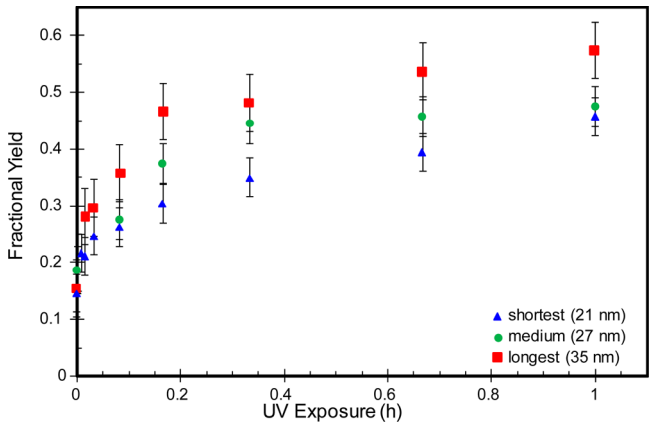

Figure 11. Fractional yield of ketene product during acetaldehyde TPD (5 L dose) as a function of UV exposure and B-TiO_2 nanorod length.

displays the fractional yield of ketene as a function of the UV exposure during CH_3CHO TPD (5 L dose at 165 K) for 21, 27, and 35 nm B-TiO_2 nanorod thin-film samples. These data reveal a clear trend of increasing ketene yield with increasing nanorod length. For example, for 0.17 h UV illumination, the ketene fractional yield for the 35 nm rods increased by more than a factor of 3 compared to that obtained with no UV illumination, while for the 21 nm rods the increases was only approximately 2-fold. Therefore, these results along with those described above for the photocoupling of CH_3OH to methyl formate provide strong evidence for a dependence of photocatalytic activity on nanorod length.

4. DISCUSSION

In this study, we have investigated the thermal and photoreactivity of simple oxygenates on the brookite-phase of TiO_2 as well as how crystallite size and shape, or more specifically nanorod length, affects photocatalytic activity. Not surprisingly, the overall thermal reactivity of the brookite nanorods toward small oxygenates was found to be similar to that reported previously for the anatase and rutile polymorphs of TiO_2.[17,18] Methanol was found to adsorb dissociatively on 5-fold coordinated Ti cations on B-TiO_2 nanorod surfaces at relatively low temperatures, and upon heating, the primary reaction pathway was recombination to produce CH_3OH, which desorbs between 190 and 450 K. In a competing pathway, the surface hydroxyl groups formed by CH_3OH dissociation react to produce water, which results in some of the methoxide groups remaining on the surface to higher temperatures. On all three polymorphs, near 640 K these methoxide groups undergo disproportionation to produce formaldehyde and molecular CH_3OH and deoxygenation to produce methane. On A-TiO_2 and R-TiO_2, bimolecular coupling of methoxide groups to produce dimethyl ether also occurs near 640 K, at least on some surfaces.[2,14] Previous studies have shown that exposed 4-

DOI: 10.1021/acs.jpcc.7b02615
J. Phys. Chem. C 2017, 121, 11488−11498

fold coordinate Ti cations which can accommodate two methoxide groups are the active sites for this reaction.[2,14] It is noteworthy that the B-TiO_2 nanorods exhibited very low activity for this coupling pathway, as illustrated in Figure 4, thus indicating that their surfaces contain few such sites. While it is apparent from the results obtained in the present study that the B-TiO_2 nanorod surfaces expose predominantly 5-fold coordinated Ti cations, the high fractional yield of methane suggests that they also contain a high population of surface oxygen vacancies.

For CH_3CHO, the primary reaction product on the B-TiO_2 nanorods was crotonaldehyde, which was produced at 460 K during TPD. This pathway also occurs on the other TiO_2 polymorphs, and its mechanism has been well-studied.[7,32−36] These previous studies have shown that CH_3CHO adsorbs on exposed Ti cations which act as Lewis acid sites, through interaction of one of the electron lone pairs of the carbonyl oxygen.[33,36] Aldol condensation of these adsorbed species to produce crotonaldehyde is catalyzed by nearby lattice oxygens, which act as Lewis base sites for abstraction of an alpha-hydrogen.[32] As a result, this reaction readily occurs on fully oxidized TiO_2, regardless of faceting; therefore, it is not surprising that it also occurs on the brookite nanorods.[7,32−36]

In addition to aldol condensation to produce crotonaldehyde, CH_3CHO adsorbed on the B-TiO_2 nanorods undergoes reductive coupling to produce butene:

$$2CH_3CHO_{(a)} \rightarrow CH_3CH = CHCH_3 + 2O_{(l)} \quad (1)$$

where $O_{(l)}$ represents lattice oxygen. On R-TiO_2, this pathway is thought to occur at oxygen vacancy sites.[7,34,38] Thus, the production of butene on the nanorods also suggests that the B-TiO_2 surface is highly defective, which is consistent with the large methane yield observed during CH_3OH TPD.

Trace amounts of crotyl alcohol and butadiene were also produced and are likely due to further reaction of the crotonaldehyde and butene products. This conclusion is consistent with the observation that they are both produced at temperatures slightly higher than those of their parent molecules (see Figure 5a). The only other significant product from CH_3CHO was ketene, which desorbed at 630 K during TPD. As will be discussed below, this product can be assigned to decomposition of adsorbed acetate species. Thus, a fraction of the adsorbed CH_3CHO reacts with surface lattice oxygen to produce adsorbed acetate.

For CH_3COOH, the TPD results displayed in Figure 7 demonstrate that this molecule adsorbs dissociatively on the B-TiO_2 nanorods at low temperatures to produce acetate intermediates which decompose upon heating to produce primarily ketene at 630 K. This result is similar to that reported by Kim and Barteau for A-TiO_2(001) single-crystal surfaces and A-TiO_2 powders.[10,37] As previously mentioned, the saturation coverage of acetate species, 1.1 molecules nm^{-2}, obtained from our TGA measurements was approximately half that for CH_3OH, suggesting that acetate species bond in a bridging configuration between two adjacent Ti cations on the surface of the B-TiO_2 nanorods. Previous studies of the other titania polymorphs also conclude that CH_3COOH adsorbs dissociatively, forming acetate intermediates with a bridging configuration on surfaces that contain only 5-fold coordinated Ti cations and/or in a bidentate structure on a single cation on surfaces that contain 4-fold coordinated Ti cations.[39,40]

The brookite nanorods exhibited photocatalytic activity similar to that reported for the anatase and rutile phases.[5,13−15,19] For example, as shown in Figure 3b, upon exposure to UV light, CH_3OH undergoes photocoupling to yield methyl formate which desorbs at 280 K during subsequent TPD. It has previously been reported that the mechanism for this reaction on both R-TiO_2 and A-TiO_2 is as follows:[41,42]

$$CH_3OH_{(Ti)} \xrightarrow{h\nu} CH_3O_{(Ti)} + H_{(O)} \quad (2)$$

$$CH_3O_{(Ti)} \xrightarrow{h\nu} CH_2O_{(Ti)} + H_{(O)} \quad (3)$$

$$CH_2O_{(Ti)} + CH_3O_{(Ti)} \xrightarrow{h\nu} HCOOCH_{3(Ti)} + H_{(O)} \quad (4)$$

In this pathway, the reaction proceeds in a stepwise fashion in which methoxy groups, which presumably could be produced thermally or photochemically, are photo-oxidized to CH_2O, followed by the photocross coupling of adsorbed CH_2O and CH_3O species to produce $HCOOCH_3$. The second step (eq 3) has been demonstrated experimentally and via ab initio calculations to be the primary photo-oxidation pathway for methoxy on the R-TiO_2(110) surface.[43] The final step, however, is not consistent with the results of the present study or those from our recent study of photocoupling of CH_3OH on A-TiO_2 nanocrystals.[13] In both cases it was observed that on surfaces that contain only adsorbed methoxy groups and no molecular methanol (see top panel in Figure 9), a low-temperature photocoupling pathway that produces $HCOOCH_3$ does not occur. We therefore propose the following alternative for the third step in the mechanism in which the photocross coupling reaction involves molecularly adsorbed CH_3OH rather than methoxide:

$$CH_2O_{(Ti)} + CH_3OH_{(Ti)} \xrightarrow{h\nu} HCOOCH_{3(Ti)} + 2H_{(O)} \quad (5)$$

An intriguing aspect of the photoinduced reactions of CH_3OH on the B-TiO_2 nanorods is that in addition to the aforementioned pathway for the production of $HCOOCH_3$ which can occur at low temperatures, another pathway was observed that produces an intermediate that reacts at 580 K to produce $HCOOCH_3$ during TPD. This pathway has not been observed for either A-TiO_2 or R-TiO_2 surfaces.[5,6] As shown in Figure 9, the intensity of this high-temperature $HCOOCH_3$ peak increased with UV exposure but was insensitive to the presence or absence of molecularly adsorbed CH_3OH on the surface. While additional study is needed to definitively determine the reaction pathway that leads to this product, one likely scenario is that a portion of the adsorbed methoxide groups is oxidized to formate during UV exposure at low temperature, and these species subsequently react with adsorbed methoxide groups to produce $HCOOCH_3$ at 580 K. Previous studies have shown that formic acid readily dissociates on R-TiO_2(110) to give formate species which are stable up to ~600 K.[44,45] Thus, reaction of formate species with adsorbed methoxide groups on the B-TiO_2 nanorods at 580 K is plausible. We therefore propose the following mechanism for this channel of $HCOOCH_3$ production:

$$CH_3O_{(Ti)} \xrightarrow{h\nu} CH_2O_{(Ti)} + H_{(O)} \quad (6)$$

$$CH_2O_{(Ti)} + O_{(l)} \xrightarrow{h\nu} HCOO_{(Ti)} + H_{(O)} \quad (7)$$

$$HCOO_{(Ti)} + CH_3O_{(Ti)} \xrightarrow{\text{heat}} HCOOCH_{3(Ti)} + O_{(l)} \quad (8)$$

DOI: 10.1021/acs.jpcc.7b02615
J. Phys. Chem. C 2017, 121, 11488−11498

As will be discussed below, the fact that the B-TiO_2 nanorods are active for the photo-oxidation of adsorbed CH_3CHO to acetate provides some additional support for this proposed mechanism. Whether this photochemical pathway for $HCOOCH_3$ production is intrinsic to B-TiO_2 or requires the specific structures present on the surface of the B-TiO_2 nanorods is an open question that cannot be answered using only the data obtained in the present study.

In contrast to CH_3OH, the primary photochemical pathway for the reaction of CH_3CHO on the B-TiO_2 nanorods is rather straightforward. As shown in Figure 5, exposure of a CH_3CHO-dosed 21 nm B-TiO_2 nanorod thin-film sample to UV light for 1 h resulted in an increase in the yield of ketene at 630 K by a factor of 5 during subsequent TPD. On the basis of the TPD results for CH_3COOH, this ketene peak can be attributed to the decomposition of adsorbed acetate intermediates. This leads to the conclusion that the B-TiO_2 nanorods are active for the photo-oxidation of adsorbed CH_3CHO to acetate. This is consistent with the reported photocatalytic activity of A-TiO_2 and R-TiO_2 which are also active this reaction.[8,46] An additional pathway that has been reported on the R-TiO_2(110) surface as well as on Degussa P25 is the photodecomposition of CH_3CHO by the ejection of a methyl radical, leaving behind an adsorbed formate species.[8,46] However, the lack of formate decomposition products CO and CO_2 from TPD following UV exposure indicates that this is not a preferred pathway on the B-TiO_2 surface.

The data in Figures 10 and 11 which show the dependence of fractional yield of TPD products resulting from photocatalytic reactions (i.e., methyl formate from CH_3OH, and ketene from CH_3CHO) on UV illumination time and nanorod length clearly show that the photocatalytic activity of the B-TiO_2 nanorods increases with rod length. This result is in accord with several previous studies of both R-TiO_2 and A-TiO_2 in which photocatalytic activity has been found to depend on both crystallite size and shape.[12−14,47−50] For example, Bennett et al. observed that the activity for the photo-oxidation of CH_3OH over A-TiO_2 nanocrystals with bipyramidal morphologies increased with particle size.[13] Similarly, Bae et al. observed that both particle size and aspect ratio affected the photocatalytic activity for CH_3CHO decomposition over R-TiO_2 nanorods.[15,51] In both of these cases, these effects were at least partially attributed to the electrons and holes preferentially migrating to different exposed crystal planes.

While preferential migration of holes and electrons to different surfaces on the B-TiO_2 nanorods (e.g., electrons to the ends and holes to the sides) possibly results in the nanorod ends and sides acting as either net-reduction or oxidation surfaces, for the high aspect ratio nanorods used in the present study changes in the length of the nanorods would not be expected to significantly impact their photocatalytic activity by altering the charge distribution on the nanorod facets. It is more likely, however, that the nanorod length affects the lifetimes of the photogenerated electrons and holes. Photo-oxidation of oxygenates (e.g., alcohols and aldehydes) on TiO_2 is generally thought to proceed via diffusion of a hole generated in the bulk to the surface, resulting in the creation of an unoccupied surface state which lies just above the valence band of the semiconductor. The migration of this hole to a surface site adjacent to the adsorbed reactant is followed by transfer of an electron from the adsorbed oxygenate to the adjacent surface hole.[52] Competing with this process is electron−hole recombination both in the bulk and with holes trapped on the surface. For A-TiO_2 thin films it has been shown that the lifetime of trapped surface holes is much longer than the time for electron transfer from an adsorbed oxygenate, thus making this process the rate-limiting step for the photo-oxidation reaction.[52] Cargnello et al. have shown using transient-absorption spectroscopy that the lifetimes of trapped surface holes increases with nanorod length for both bare and Pt-decorated B-TiO_2 nanorods. While the effect was bigger for the Pt-decorated rods where the metal particles act as trap sites for photogenerated electrons, a significant increase in the hole decay rate was still observed for the bare nanorods.[23] Because rod length is not likely to affect the rate of adsorbate−hole reaction, the increase in photocatalytic activity with B-TiO_2 nanorod length observed in the present study implies that the electron−hole recombination rate, either in the bulk or on the surface, decreases with increasing nanorod length, thereby increasing the probability that a hole will diffuse to the surface and remain long enough so it can react with an adsorbate.

A similar conclusion has been reported by Cargnello et al.[23] who studied the aqueous phase photoreforming of ethanol to produce H_2 over Pt-particle decorated B-TiO_2 nanorods (these nanorods were essentially identical to those used in the present study) and observed a strong dependence of the reaction rate on rod length. They noted that the diffusion lengths for photogenerated electrons and holes in titania are of the order of micrometers and nanometers, respectively, and that the small diffusion lengths for the holes effectively confines them to the width of the nanorods, which in our case is 5.5 nm. In contrast, for the electrons, the one-dimensional nature of the nanorods coupled with their long diffusion length allows for their delocalization along the length of the nanorod.[23,53,54] This effectively allows for a higher degree of charge separation between the electrons and holes in the longer nanorods, which in turn would decrease the electron−hole recombination rate, allowing for an increase in the concentration of holes at the nanorod surface for reaction with the adsorbed species.

5. CONCLUSIONS

The results of this study provide insight into the thermal and photochemical reactivity of the brookite phase of TiO_2 toward alcohols, aldehydes, and carboxylic acids, as well as how the interplay between nanocrystallite size and shape and the dynamics of photogenerated electrons and holes can affect photocatalytic activity. On the B-TiO_2 nanorods, CH_3OH was found to adsorb dissociatively on 5-fold coordinate Ti cations to form methoxide groups that undergo deoxygenation to produce CH_4 and dehydrogenation to produce CH_2O at temperatures between 640 and 650 K. Little activity for bimolecular coupling to produce $(CH_3)_2O$ was observed, indicating that the surfaces of the nanorods contained few 4-fold coordinate Ti cations. The primary reaction pathway for CH_3CHO on the B-TiO_2 nanorods was aldol condensation near 460 K to produce crotonaldehyde, which demonstrates the Lewis acid−base character of Ti cation−oxygen anion site pairs on the surface. Acetic acid was also found to absorb dissociatively on these site pairs to produce acetate intermediates which decompose at 630 K to produce ketene.

Studies with UV-exposed samples also showed that B-TiO_2 nanorods were active for the photocoupling of CH_3OH to produce methyl formate. Our results indicate that this reaction proceeds via photoinduced dehydrogenation of an adsorbed methoxide group to produce CH_2O which in a subsequent photocatalytic step reacts with adsorbed molecular methanol to

DOI: 10.1021/acs.jpcc.7b02615
J. Phys. Chem. C 2017, 121, 11488−11498

produce methyl formate. Photo-oxidation of methoxide groups to formate species was also observed to occur. This reaction presumably proceeds through a CH_2O intermediate. Formate species formed in this manner reacted with adsorbed methoxide groups at 580 K to produce methyl formate. The photochemical oxidation of CH_3OH to formate appears to be specific to the B-TiO_2 phase having not previously been observed for A-TiO_2 and R-TiO_2. This pathway on the B-TiO_2 nanorods is also consistent with what was observed for CH_3CHO, which underwent photo-oxidation to acetate on the nanorods.

Lastly, studies of the photochemical oxidation activity of the B-TiO_2 nanorods showed that photoactivity increased with increasing nanorod length. This was most apparent for the photo-oxidation of CH_3CHO to acetate where the yield of the acetate decomposition product, ketene, during TPD runs following UV exposure was markedly higher for the 35 nm nanorods compared to that of the 21 nm nanorods. A similar although less pronounced dependence on nanorod length was also observed for the photocoupling of methanol to methyl formate. We attribute this increase in photoactivity with nanorod length to enhanced delocalization of the excited electrons in the longer rods, thereby decreasing the rate of electron−hole recombination, which increases the probability that holes will diffuse to the surface and react with an adsorbed species.

■ ASSOCIATED CONTENT

Supporting Information

The Supporting Information is available free of charge on the ACS Publications website at DOI: 10.1021/acs.jpcc.7b02615.

B-TiO_2 nanorod characterization (XPS spectra), powder system TPD/TGA data, and high-temperature $HCOOCH_3$ TPD fractional yield data (PDF)

■ AUTHOR INFORMATION

Corresponding Authors

*E-mail: pepinp@seas.upenn.edu. Tel: 215-898-7230.
*E-mail: vohs@seas.upenn.edu. Tel: 215-898-6318.

ORCID

Benjamin T. Diroll: 0000-0003-3488-0213
John M. Vohs: 0000-0002-8283-5241

Present Address

‖B.T.D.: Center for Nanoscale Materials, Argonne National Laboratory, Lemont, IL 60439.

Notes

The authors declare no competing financial interest.

■ ACKNOWLEDGMENTS

Funding for this study was provided by the U.S. Department of Energy, Office of Science, Office of Basic Energy Sciences under Grant DEFG02-04ER15605.

■ REFERENCES

(1) Kim, K. S.; Barteau, M. A.; Farneth, W. E. Adsorption and Decomposition of Aliphatic-Alcohols on TiO_2. *Langmuir* **1988**, *4*, 533−543.

(2) Kim, K. S.; Barteau, M. A. Reactions of Methanol on TiO_2 (001) Single-Crystal Surfaces. *Surf. Sci.* **1989**, *223*, 13−32.

(3) Henderson, M. A.; Otero-Tapia, S.; Castro, M. E. The Chemistry of Methanol on the Surface: the TiO_2 (110) Influence of Vacancies and Coadsorbed Species. *Faraday Discuss.* **1999**, *114*, 313−329.

(4) Shen, M. M.; Henderson, M. A. Identification of the Active Species in Photochemical Hole Scavenging Reactions of Methanol on TiO_2. *J. Phys. Chem. Lett.* **2011**, *2*, 2707−2710.

(5) Phillips, K. R.; Jensen, S. C.; Baron, M.; Li, S. C.; Friend, C. M. Sequential Photo-oxidation of Methanol to Methyl Formate on TiO_2 (110). *J. Am. Chem. Soc.* **2013**, *135*, 574−577.

(6) Yuan, Q.; Wu, Z. F.; Jin, Y. K.; Xu, L. S.; Xiong, F.; Ma, Y. S.; Huang, W. X. Photocatalytic Cross-Coupling of Methanol and Formaldehyde on a Rutile TiO_2 (110) Surface. *J. Am. Chem. Soc.* **2013**, *135*, 5212−5219.

(7) Idriss, H.; Kim, K. S.; Barteau, M. A. Carbon Carbon Bond Formation Via Aldolization of Acetaldehyde on Single-Crystal and Polycrystalline TiO_2 Surfaces. *J. Catal.* **1993**, *139*, 119−133.

(8) Zehr, R. T.; Henderson, M. A. Acetaldehyde Photochemistry on TiO_2 (110). *Surf. Sci.* **2008**, *602*, 2238−2249.

(9) Tanner, R. E.; Liang, Y.; Altman, E. I. Structure and Chemical Reactivity of Adsorbed Carboxylic Acids on Anatase TiO_2 (001). *Surf. Sci.* **2002**, *506*, 251−271.

(10) Kim, K. S.; Barteau, M. A. Structure and Composition Requirements for Deoxygenation, Dehydration, and Ketonization Reactions of Carboxylic-Acids on TiO_2 (001) Single-Crystal Surfaces. *J. Catal.* **1990**, *125*, 353−375.

(11) Tao, J. G.; Luttrell, T.; Bylsma, J.; Batzill, M. Adsorption of Acetic Acid on Rutile TiO_2 (110) vs (011)-2 × 1 Surfaces. *J. Phys. Chem. C* **2011**, *115*, 3434−3442.

(12) Ohno, T.; Sarukawa, K.; Matsumura, M. Crystal Faces of Rutile and Anatase TiO_2 Particles and their Roles in Photocatalytic Reactions. *New J. Chem.* **2002**, *26*, 1167−1170.

(13) Bennett, D. A.; Cargnello, M.; Gordon, T. R.; Murray, C. B.; Vohs, J. M. Thermal and Photochemical Reactions of Methanol on Nanocrystalline Anatase TiO_2 Thin Films. *Phys. Chem. Chem. Phys.* **2015**, *17*, 17190−17201.

(14) Bennett, D. A.; Cargnello, M.; Diroll, B. T.; Murray, C. B.; Vohs, J. M. Shape-dependence of the Thermal and Photochemical Reactions of Methanol on Nanocrystalline Anatase TiO_2. *Surf. Sci.* **2016**, *654*, 1−7.

(15) Bae, E.; Ohno, T. Exposed Crystal Surface-controlled Rutile TiO_2 Nanorods Prepared by Hydrothermal Treatment in the Presence of Poly(vinyl pyrrolidone). *Appl. Catal., B* **2009**, *91*, 634−639.

(16) Morris Hotsenpiller, P. A.; Bolt, J. D.; Farneth, W. E.; Lowekamp, J. B.; Rohrer, G. S. Orientation Dependence of Photochemical Reactions on TiO_2 Surfaces. *J. Phys. Chem. B* **1998**, *102*, 3216−3226.

(17) Linsebigler, A. L.; Lu, G. Q.; Yates, J. T. Photocatalysis on TiO_2 Surfaces - Principles, Mechanisms, and Selected Results. *Chem. Rev.* **1995**, *95*, 735−758.

(18) Diebold, U. The Surface Science of Titanium Dioxide. *Surf. Sci. Rep.* **2003**, *48*, 53−229.

(19) Henderson, M. A. A Surface Science Perspective on TiO_2 Photocatalysis. *Surf. Sci. Rep.* **2011**, *66*, 185−297.

(20) Li, J. G.; Tang, C. C.; Li, D.; Haneda, H.; Ishigaki, T. Monodispersed Spherical Particles of Brookite-type TiO_2: Synthesis, Characterization, and Photocatalytic Property. *J. Am. Ceram. Soc.* **2004**, *87*, 1358−1361.

(21) Murakami, N.; Kamai, T.; Tsubota, T.; Ohno, T. Novel Hydrothermal Preparation of Pure Brookite-type Titanium(IV) Oxide Nanocrystal Under Strong Acidic Conditions. *Catal. Commun.* **2009**, *10*, 963−966.

(22) Ohno, T.; Higo, T.; Saito, H.; Yuajn, S.; Jin, Z. Y.; Yang, Y.; Tsubota, T. Dependence of Photocatalytic Activity on Aspect Ratio of a Brookite TiO_2 Nanorod and Drastic Improvement in Visible Light Responsibility of a Brookite TiO_2 Nanorod by Site-selective Modification of Fe^{3+} on Exposed Faces. *J. Mol. Catal. A: Chem.* **2015**, *396*, 261−267.

(23) Cargnello, M.; et al. Engineering Titania Nanostructure to Tune and Improve its Photocatalytic Activity. *Proc. Natl. Acad. Sci. U. S. A.* **2016**, *113*, 3966−3971.

(24) Buonsanti, R.; Grillo, V.; Carlino, E.; Giannini, C.; Kipp, T.; Cingolani, R.; Cozzoli, P. D. Nonhydrolytic Synthesis of High-quality

DOI: 10.1021/acs.jpcc.7b02615
J. Phys. Chem. C 2017, 121, 11488−11498

Anisotropically Shaped Brookite TiO_2 Nanocrystals. *J. Am. Chem. Soc.* **2008**, *130*, 11223−11233.
(25) Gordon, T. R.; Cargnello, M.; Paik, T.; Mangolini, F.; Weber, R. T.; Fornasiero, P.; Murray, C. B. Nonaqueous Synthesis of TiO_2 Nanocrystals Using TiF_4 to Engineer Morphology, Oxygen Vacancy Concentration, and Photocatalytic Activity. *J. Am. Chem. Soc.* **2012**, *134*, 6751−6761.
(26) Diebold, U.; Madey, T. TiO_2 by XPS. *Surf. Sci. Spectra* **1996**, *4*, 227−231.
(27) Dana, J. D.; Dana, E. S.; Gaines, R. V. *Dana's New Mineralogy: The System of Mineralogy of James Dwight Dana and Edward Salisbury Dana*, 8th ed.; Wiley: New York, 1997.
(28) Carrizosa, I.; Munuera, G. Study of Interaction of Aliphatic-Alcohols with TiO_2 0.2. Mechanism of Alcohol Dehydration on Anatase. *J. Catal.* **1977**, *49*, 189−200.
(29) Carrizosa, I.; Munuera, G.; Castanar, S. Study of Interaction of Aliphatic-Alcohols with TiO_2 0.3. Formation of Alkyl-Titanium Species during Methanol Decomposition. *J. Catal.* **1977**, *49*, 265−277.
(30) Lusvardi, V. S.; Barteau, M. A.; Farneth, W. E. The Effects of Bulk Titania Crystal-Structure on the Adsorption and Reaction of Aliphatic-Alcohols. *J. Catal.* **1995**, *153*, 41−53.
(31) Suda, Y.; Morimoto, T.; Nagao, M. Adsorption of Alcohols on Titanium-Dioxide (Rutile) Surface. *Langmuir* **1987**, *3*, 99−104.
(32) Idriss, H.; Barteau, M. A. Selectivity and Mechanism Shifts in the Reactions of Acetaldehyde on Oxidized and Reduced TiO_2 (001) Surfaces. *Catal. Lett.* **1996**, *40*, 147−153.
(33) Rekoske, J. E.; Barteau, M. A. Competition between Acetaldehyde and Crotonaldehyde during Adsorption and Reaction on Anatase and Rutile Titanium Dioxide. *Langmuir* **1999**, *15*, 2061−2070.
(34) Luo, S. C.; Falconer, J. L. Acetone and Acetaldehyde Oligomerization on TiO_2 Surfaces. *J. Catal.* **1999**, *185*, 393−407.
(35) Luo, S. C.; Falconer, J. L. Aldol Condensation of Acetaldehyde to form High Molecular Weight Compounds on TiO_2. *Catal. Lett.* **1999**, *57*, 89−93.
(36) Rasko, J.; Kiss, J. Adsorption and Surface Reactions of Acetaldehyde on TiO_2, CeO_2 and Al_2O_3. *Appl. Catal., A* **2005**, *287*, 252−260.
(37) Kim, K. S.; Barteau, M. A. Pathways for Carboxylic-Acid Decomposition on TiO_2. *Langmuir* **1988**, *4*, 945−953.
(38) Idriss, H.; Pierce, K.; Barteau, M. A. Carbonyl Coupling on the TiO_2 (001) Surface. *J. Am. Chem. Soc.* **1991**, *113*, 715−716.
(39) Manzhos, S.; Giorgi, G.; Yamashita, K. A Density Functional Tight Binding Study of Acetic Acid Adsorption on Crystalline and Amorphous Surfaces of Titania. *Molecules* **2015**, *20*, 3371−3388.
(40) Guo, Q.; Cocks, I.; Williams, E. M. The Orientation of Acetate on a TiO_2 (110) Surface. *J. Chem. Phys.* **1997**, *106*, 2924−2931.
(41) Xu, C. B.; Yang, W. S.; Guo, Q.; Dai, D. X.; Chen, M. D.; Yang, X. M. Molecular Hydrogen Formation from Photocatalysis of Methanol on Anatase-TiO_2 (101). *J. Am. Chem. Soc.* **2014**, *136*, 602−605.
(42) Guo, Q.; Xu, C. B.; Yang, W. S.; Ren, Z. F.; Ma, Z. B.; Dai, D. X.; Minton, T. K.; Yang, X. M. Methyl Formate Production on TiO_2 (110), Initiated by Methanol Photocatalysis at 400 nm. *J. Phys. Chem. C* **2013**, *117*, 5293−5300.
(43) Kolesov, G.; Vinichenko, D.; Tritsaris, G. A.; Friend, C. M.; Kaxiras, E. Anatomy of the Photochemical Reaction: Excited-State Dynamics Reveals the C-H Acidity Mechanism of Methoxy Photo-oxidation on Titania. *J. Phys. Chem. Lett.* **2015**, *6*, 1624−1627.
(44) Kim, K. S.; Barteau, M. A. Structural Dependence of the Selectivity of Formic-Acid Decomposition on Faceted TiO_2 (001) Surfaces. *Langmuir* **1990**, *6*, 1485−1488.
(45) Henderson, M. A. Complexity in the Decomposition of Formic Acid on the TiO_2 (110) Surface. *J. Phys. Chem. B* **1997**, *101*, 221−229.
(46) Muggli, D. S.; McCue, J. T.; Falconer, J. L. Mechanism of the Photocatalytic Oxidation of Ethanol on TiO_2. *J. Catal.* **1998**, *173*, 470−483.
(47) Chen, W.; Kuang, Q.; Wang, Q. X.; Xie, Z. X. Engineering a High Energy Surface of Anatase TiO_2 Crystals towards Enhanced Performance for Energy Conversion and Environmental Applications. *RSC Adv.* **2015**, *5*, 20396−20409.
(48) Murakami, N.; Kurihara, Y.; Tsubota, T.; Ohno, T. Shape-Controlled Anatase Titanium(IV) Oxide Particles Prepared by Hydrothermal Treatment of Peroxo Titanic Acid in the Presence of Polyvinyl Alcohol. *J. Phys. Chem. C* **2009**, *113*, 3062−3069.
(49) D'Arienzo, M.; Carbajo, J.; Bahamonde, A.; Crippa, M.; Polizzi, S.; Scotti, R.; Wahba, L.; Morazzoni, F. Photogenerated Defects in Shape-Controlled TiO_2 Anatase Nanocrystals: A Probe To Evaluate the Role of Crystal Facets in Photocatalytic Processes. *J. Am. Chem. Soc.* **2011**, *133*, 17652−17661.
(50) Liu, C.; Han, X. G.; Xie, S. F.; Kuang, Q.; Wang, X.; Jin, M. S.; Xie, Z. X.; Zheng, L. S. Enhancing the Photocatalytic Activity of Anatase TiO_2 by Improving the Specific Facet-Induced Spontaneous Separation of Photogenerated Electrons and Holes. *Chem. - Asian J.* **2013**, *8*, 282−289.
(51) Bae, E.; Murakami, N.; Ohno, T. Exposed Crystal Surface-controlled TiO_2 Nanorods having Rutile Phase from $TiCl_3$ under Hydrothermal Conditions. *J. Mol. Catal. A: Chem.* **2009**, *300*, 72−79.
(52) Tamaki, Y.; Furube, A.; Murai, M.; Hara, K.; Katoh, R.; Tachiya, M. Direct Observation of Reactive Trapped Holes in TiO_2 Undergoing Photocatalytic Oxidation of Adsorbed Alcohols: Evaluation of the Reaction Rates and Yields. *J. Am. Chem. Soc.* **2006**, *128*, 416−417.
(53) Zhu, K.; Vinzant, T. B.; Neale, N. R.; Frank, A. J. Removing Structural Disorder from Oriented TiO_2 Nanotube Arrays: Reducing the Dimensionality of Transport and Recombination in Dye-sensitized Solar Cells. *Nano Lett.* **2007**, *7*, 3739−3746.
(54) Varghese, O. K.; Paulose, M.; Grimes, C. A. Long Vertically Aligned Titania Nanotubes on Transparent Conducting Oxide for Highly Efficient Solar Cells. *Nat. Nanotechnol.* **2009**, *4*, 592−597.

DOI: 10.1021/acs.jpcc.7b02615
J. Phys. Chem. C 2017, 121, 11488−11498